Astronomical and Astrophysical Transactions (*AApTr*), 2016, Vol. 29, Issue 2, pp. 143–164,
ISSN 1055-6796, Photocopying permitted by license only, ©Cambridge Scientific Publishers

MASTER and unsolved GRB observational and theoretical problems

V.M. Lipunov*

Lomonosov Moscow State University, Sternberg Astronomical Institute, Universitetsky pr. 13, 119991, Russia

Received 25 April, 2016

The observations of GRBs over many years are discussed. The main key steps in GRB investigations are the following: the first simultaneous observations of GRB720117 (Cosmos-461 and Vela); the first bimodal distribution's discussion in 1981 by Mazets, Golenetskii; the first GRB with optical afterglow investigations GRB970228 (BATSE); the first prompt observations of GRB by Akerlof (GRB990123, ROTSE-I response to BATSE alert) are demonstrated. The evolution of the coalescence rate of double neutron stars and neutron star–black hole binaries were first computed by Lipunov et al. in 1995. We also discuss scenarios for long and short GRBs. And there are some results of MASTER Global Robotic Net GRB observations.

Keywords: Gamma ray bursts (GRBs), theory, observations, MASTER

1 The first key steps in GRB investigations

The gamma-ray burst (GRB) investigations started at the end of 1960s. A search for reports of a nova or supernova within a reasonable time of first registered GRBs was made by Klebesadel et al. (1973) with 16 GRBs, observed by Vela satellites, and the lack of correlation between GRBs and nova and supernova was reported. GRB670702 is one of the first registered GRBs (Strong et al. 1974) (Fig. 1).

Mazets et al. (1974) reported the results of the simultaneous observation of GRB720117 by satellites Cosmos-461 and Vela, which provided the proof that GRB came from galactic or metagalactic source (i.e. not from the earth, for which policy Vela were launched). Mazets, Golenetskii (1981), Mazets (1988) wrote about the isotropy and bimodal distribution of known GRBs, and this was confirmed more than 10 years later by the 1000 BATSE GRB distribution analysis (Fig. 2).

*Email: lipunov2007@gmail.com

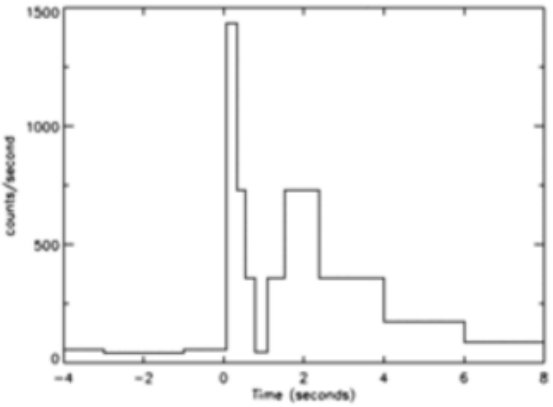


Figure 1 GRB670702. One of the first registered GRBs.

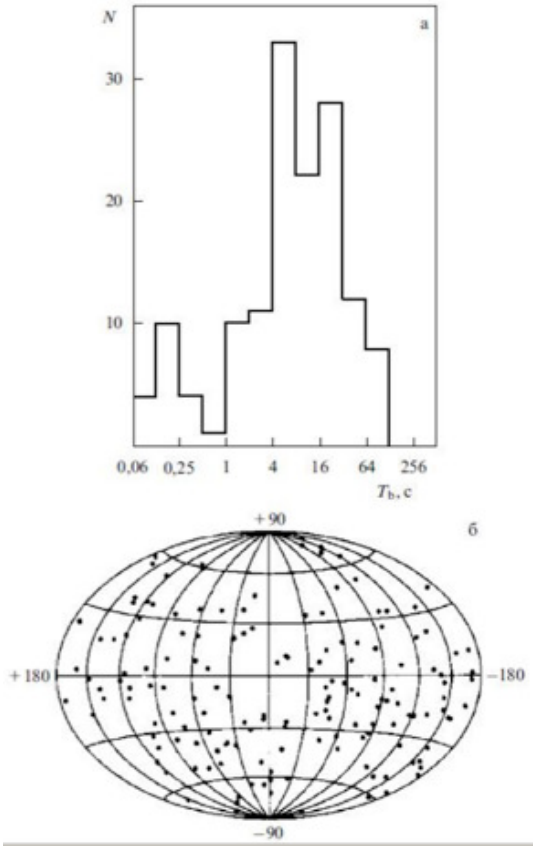


Figure 2 The bimodal distribution of known GRBs by time duration and the distribution of the GRB sources on the sky using the observations in KONUS and VENERA experiments from 1978 up to 1983. T_b is the time duration of GRB, N is the number of events (Mazets, Golenetskii 1981, 1988; Aptekar et al. 2010). Both results later were confirmed by BATSE 1000 GRB distribution.

2 Possible scenario

The evolution of the double neutron star merging rate and the cosmological origin of gamma-ray burst sources were first described by Lipunov et al. (1995).

The evolution of the coalescence rate of double neutron stars (NSs) and neutron star–black hole (BH) binaries were first computed by Lipunov et al. (1995) for the model galaxies with different star formation rates. Assuming that gamma-ray bursts (GRBs) originate from NS + NS or NS + BH merging in distant galaxies, theoretical $\log N$–$\log S$ distributions for GRBs were calculated (Fig. 3) for the first time taking the computed merging rates into account. We use a flat cosmological model with different values of the cosmological constant A and under various assumptions about the star formation history in galaxies. The calculated source evolution predicts a 5–10 times increase of the source statistics at count rates 3–10 times lower than the existing BATSE sensitivity limit. The most important parameter in fitting the second BATSE catalog is the initial redshift of star formation, which is found to be $z^* = 2$–5, depending on a poorly determined average spectral index of GRBs.

In February 1997 BATSE registered the key gamma-ray burst GRB 970228 (Costa et al. 1997), which was first proved by optical observations (Groot et al. 1997a,b; Kulkarni et al. 1997). The redshift was $z = 0.695$ (Bloom et al. 2001).

The following GRB 970508's (Bond et al. 1997) optical transient within the error box of the gamma ray burst GRB 970508 was imaged 4 hours after the event (Castro-Tirado 1997). It displayed a strong ultraviolet excess, and reached maximum brightness 2 days later. The optical spectra did not show any emission lines, and no variations on time scales of minutes were observed for 1 hour during the decline phase. According to the fireball and afterglow models, the intensity should rise mono-

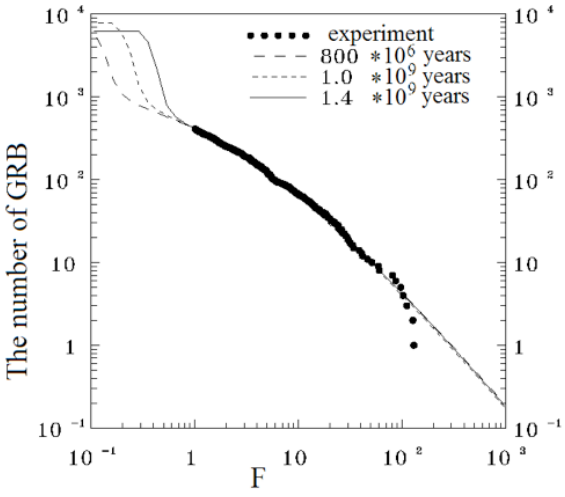


Figure 3 A $\log N$–$\log S$ diagram simulated for the sources evolving in a flat cosmological model with the best-fit vacuum energy $\Omega_\Lambda = 0.75$. There are the points from the second BATSE catalog (GRB distribution), see Lipunov et al. (1995).

tonically before the observed optical maximum, but the data indicate that another physical mechanism may be responsible for the constant phase seen during the first hours after the burst.

After the BeppoSAX launch the rapid availability of precise coordinates for the bursts allowed the detection of faint optical and radio afterglows – optical spectra thus obtained have demonstrated conclusively that the bursts occur at cosmological distances. But despite efforts by several groups, optical detection has not hitherto been achieved during the brief duration of a burst. The cosmological nature of GRB was proved, but all these observations were not prompt before GRB990123. There was the afterglow that could give us the possibility to measure the redshift for the host galaxy, but gave us no information about the work of the central machine.

The origin of gamma-ray bursts has been enigmatic since the discovery of the optical prompt (simultaneous with gamma) emission discovery of GRB 990123 by Akerlof et al. (1999a,b) with ROTSE-I project (Akerlof et al. 2000), see Fig. 4.

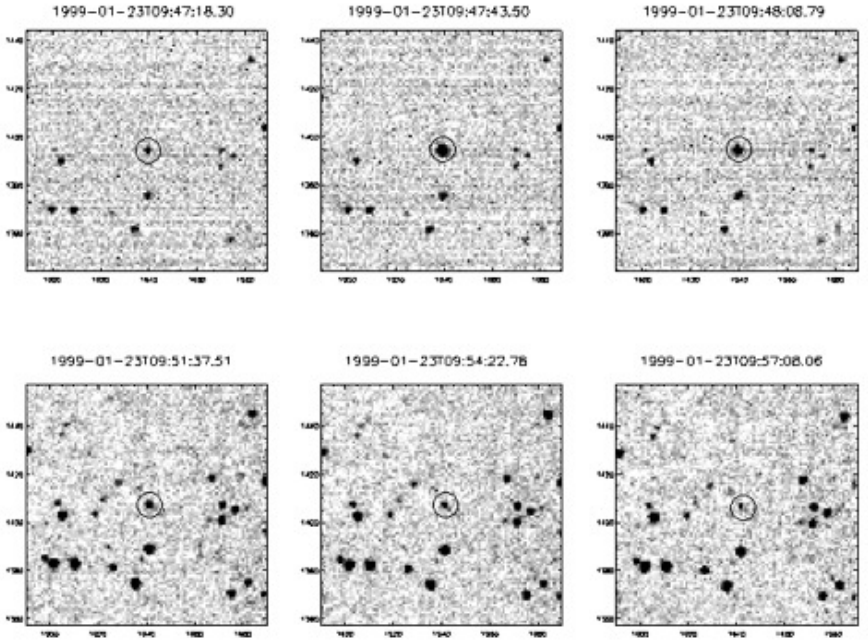


Figure 4 The first GRB with prompt optical emission GRB 990123, that was detected by Akerlof in 1999 in ROTSE experiment.

3 Unsolved GRB observational and theoretical problems

The typical GRB energy is $E \sim 10^{51–53}$ erg. Typical collapse gives $E \sim 0.1Mc^2$, where collapsing mass is $M \sim 1$–10 solar masses. The two most popular suggestions

to explain GRB were the following: the neutron star merging (Bisnovatyi-Kogan, Blinnikov, Zaharov 1984) and the collapse (Paczynski 1986).

The spectrum has maximum of energy at $E_{\rm peak} \sim 1$ MeV. The typical collapse temperature is $T \sim 2m_{\rm e}c^2 \sim 10^{10}$ K ~ 1 MeV, where $m_{\rm e}$ is mass of electron, c is speed of light. Observed event duration is $\Delta t_{\rm obs} \sim 0.1$–100 s. The typical collapse time $\Delta t \sim R_{\rm g}/c \sim 10^{-5}$ s $\ll \Delta t_{\rm obs}$.

Characteristic time of the magneto-rotational collapse is:

$$\Delta T \sim I\omega/K,$$

where I is the moment of inertia, ω is angular velocity, K is magnetic force moment, $\Delta T \sim R^2/D$, R is characteristic size of disc-like body, D is diffusion coefficient, $D \sim$ viscosity.

There are two scenarios for the **long GRB**:

1. Woosley (1993) Scenario. The gamma-ray bursts from stellar mass accretion disks around black holes can be a result of:

1a. Core collapse means the black hole formation from the massive star;

1b. Formation of a massive accretion disk;

1c. GRB is the result of accretion in massive disk (Blandford–Znajek mechanism).

2. Spinar Scenario. Electron–positron collapse of highly massive ($M \sim 100$ solar masses) fast rotating stars:

2a. Spinar formation due to centrifugal barrier (precursor stage);

2b. Extreme Kerr black hole formation (GRB stage).

There are two possible scenarios for the **short GRB**:

1. Woosley Scenario with Core collapse of the massive star, but this scenario does not work.

2. Spinar Scenario (NS + NS) merging:

2a. Spinar formation (precursor stage);

2b. Extreme Kerr black hole formation (GRB stage).

The importance of the magnetic rotational effect was first pointed out with reference to the energetics and evolution of the quasars (Hoyle, Fowler 1963a,b; Ozernoy 1966; Morrison 1969; Ozernoy, Usov 1973) and SN explosion (Bisnovatyi-Kogan 1971; LeBlanc, Wilson 1970).

The formation of the quasi equilibrium object was called Spinar. Lipunov (1983) proposed the idea of Spinar with stellar mass (see Ostriker 1973). Spin-up and spin-down was considered by Lipunov (1987) in the frame of the magneto rotator. The relativistic Spinar was considered by Lipunova (1997), and noted for the first time the model of GRB as the Spinar.

Prolongated GRB activity, i.e. formation of a gravitationally bound object after binary neutron star merging and GRB phenomena, was predicted in two papers: by Lipunova (1997) and in Lipunova, Lipunov (1998), where the stages that follow the merging of two neutron stars were discussed.

The hypothesis was discussed as to whether the residual optical emission of the gamma-ray bursts is pulsar-like and its evolution driven by magneto dipole energy losses. It is shown that binary neutron star merging can be accompanied by two

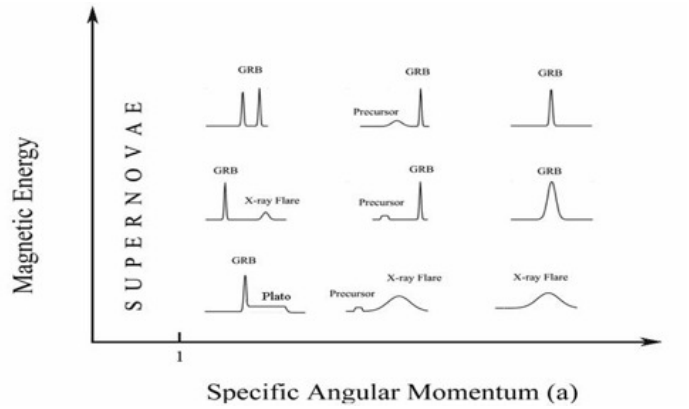


Figure 5 Classification of GRBs and surrounding events in terms of the spinar paradigm. In the case of a weak magnetic field and large angular momentum (the bottom right curve) the first burst is weak (because of the high centrifugal barrier) and soft. It is followed by slow collapse (magnetic field is weak), which results in a weak X-ray burst. In the case of small angular momentum (the bottom left curve) the energy released at the centrifugal barrier is large and the burst appears as a gamma-ray burst, whereas the second burst, which corresponds to the collapse of the spinar, is again weak and soft and shows up as a distant X-ray burst. In the case of an even weaker magnetic field the second flare behaves as an extralong X-ray plateau. In the case of stronger magnetic field the flare becomes more like a gamma-ray burst, its energy increases and the flare itself becomes part of a gamma-ray burst (the top left curve). As we move rightward, the angular momentum increases and the first flare loses its energy to become a close precursor of the second flare, which in the case of a strong magnetic field becomes a powerful gamma-ray burst. The collapse of a core with the effective Kerr parameter smaller than unity results in a supernova explosion, see Lipunov, Gorbovskoy (2007).

gravitational wave bursts separated either by the time of spinar's collapse $t_{\rm spin}$ or neutron star cooling time ($\sim$10 s), depending on the masses of neutron stars.

An Extra Long X-Ray Plateau in a Gamma-Ray Burst and the Spinar Paradigm was discussed first by Lipunov, Gorbovskoy (2007), see Figs. 5 and 6. The discovered gamma-ray burst GRB 070110 displayed an extraordinary X-ray afterglow with X-ray radiation, i.e. an X-ray plateau observed for 20,000 s. The observed properties of the plateau can be naturally interpreted in terms of the model with a spinar – a quasi-equilibrium collapsing object whose equilibrium is maintained by the balance of centrifugal and gravitational forces and whose evolution is determined by its magnetic field. If this model is true, then for 1 hr, the Swift X-ray telescopes recorded radiation from an object with a size smaller than the Schwarzschild radius.

The nonstationary relativistic pseudo-Newtonian Spinar Model was introduced by Lipunov, Gorbovskoy (2008). A spinar is a collapsing object with quasi-equilibrium. Its equilibrium is maintained by the balance of centrifugal and gravitational forces and its evolution is determined by its magnetic field. A model of spinar quasi-equilibrium has recently been discussed in the context of an extralong X-ray plateau in a gamma-ray burst. We proposed a simple non-stationary three-parameter collapse model with the determining role of rotation and magnetic field. The input parameters of the

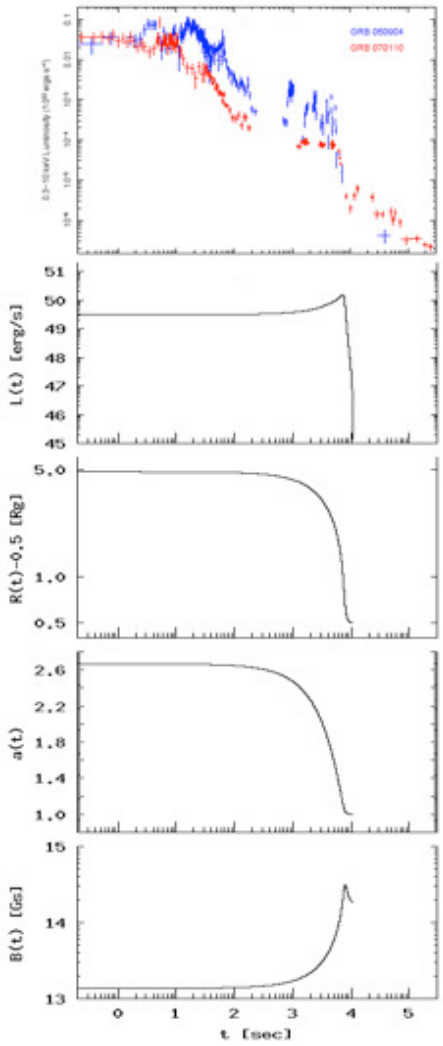


Figure 6 Among the several hundreds of gamma-ray bursts, the GRB070110 and GRB050904 do not fit into the usual picture of the X-ray afterglow formation. Both bursts have a long plateau lasting up to 6000–7000 seconds in the rest frame. The rest-frame light curve of the gamma-ray bursts GRB 070110 and GRB 050904 on the upper figure were adopted from Troja et al. (2007), who suggested that such a long display of activity is associated with features of the central engine and specifically with the formation of a neutron star after the collapse of the core of low-mass (less Oppenheimer–Volkoff limit). The other figures demonstrate the exact solution for the set of burst equations from Lipunov, Gorbovskoy (2007). There are in logarithmic scales the spinar luminosity L, radius R, effective Kerr parameter (a), and mean magnetic field B evolution with logarithm of time t.

theory are the mass, angular momentum and magnetic field of the collapsar. The model includes an approximate description of the following effects: the centrifugal force, the relativistic effects of the Kerr metrics, the pressure of nuclear matter, the

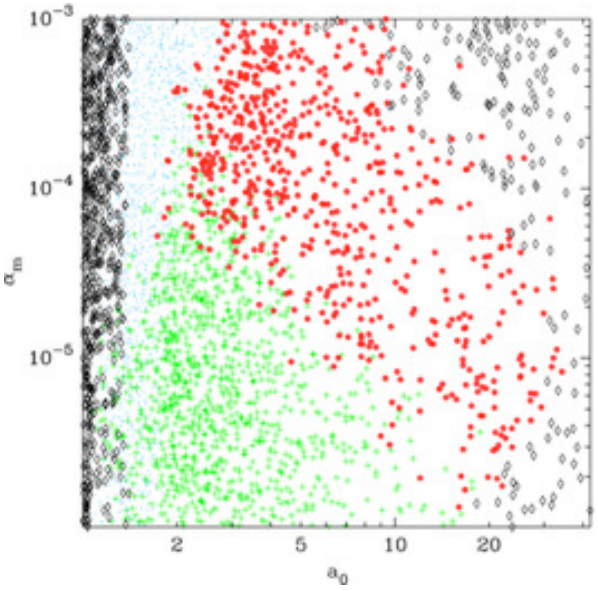


Figure 7 The magnetic parameter $\alpha_{\rm m}$ versus initial effective Kerr parameter a_0 for different classes of GRBs: with precursor (big red dots), with the stronger first peak (green pluses), single peak (black diamonds) and merged peaks (small blue dots).

dissipation of angular momentum as a result of the magnetic field, the decrease of the dipole magnetic moment as a result of compression and general-relativity effects (the black hole has no hair), neutrino cooling, time dilatation and gravitational redshift. The model describes the temporal behavior of the central engine and demonstrates the qualitative variety of the types of such behavior in nature. We applied our approach to an explanation of the observed features of all types of gamma-ray bursts. In particular, the model allows the unification of the phenomena of precursors, X-ray and optical flares, and the appearance of a plateau on the time-scale of several thousand seconds.

The evolution of close binaries and gamma-ray bursts was introduced by Bogomazov, Lipunov, Tutukov (2007). We analyzed the late stages of evolution of massive ($M_0 \gtrsim 8M_\odot$) close binaries, from the point of view of possible mechanisms for the generation of gamma-ray bursts. It is assumed that a gamma-ray burst requires the formation of a massive ($\sim 1\,M_\odot$), compact ($R \lesssim 10$ km) accretion disk around a Kerr black hole or neutron star, see Figs. 7 and 8. Such Kerr black holes are produced by core collapses of Wolf–Rayet stars in very close binaries, as well as by mergers of neutron stars and black holes or two neutron stars in binaries. The required accretion disks can also form around neutron stars that were formed via the collapse of ONeMg white dwarfs. We estimate the Galactic rate of events resulting in the formation of rapidly rotating relativistic objects. The computations were carried out using the "Scenario Machine" (Lipunov et al. 1996, 2009).

So up to this moment, there is common (more or less) opinion:
about the Short GRB as:

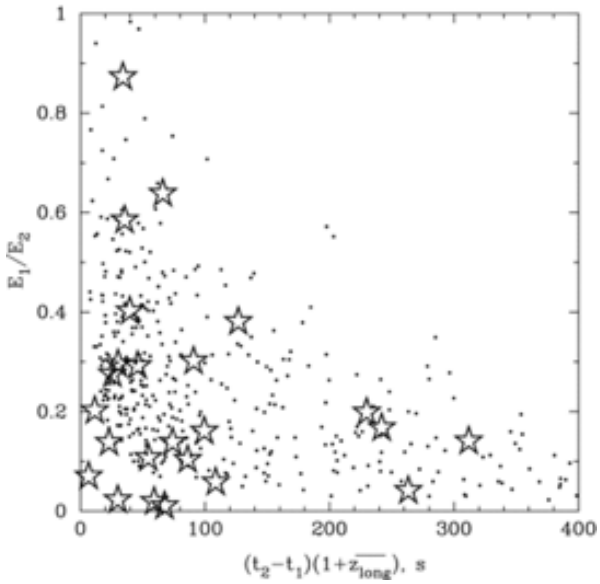


Figure 8 The ratio of the energy released during the precursor and the main peak versus separation time multiplied by the constant factor. Dots represent model results for GRBs with precursor for population '1'. The average value of the redshift for long GRBs. Stars are adopted from Fig. 13 of Koshut et al. (1995).

– the neutron stars merging
– neutron star and black hole merging;

About the Long GRBs as the massive star collapse.

Is there any new physics near GRB?

The Kardashev (1995) limit (maximal energy accelerated particles):
$(B^2/8\pi)R^3 = Mc^2$, $R = R_{\rm g} = 2GM/c^2$.
Maximal energy $= eER \sim eBR \sim (1/137)E_{\rm pl} \sim 10^{26}$ eV.

The Predictions of the Spinar Paradigm are the following:

1. The existence precursors with more than 1000 sec before GRB;
2. The existence of extra long GRB or X-ray flare;
3. We need high wave length electromagnetic prompt observations from Radio, IR, Optical to X-Ray, Gamma, UHE range for Understanding of the Central Engine.

There are five unsolved GRB optical observational problems:

1. The Discovery of most distant gravitationally bounded objects $z > 10$–12.
2. The Discovery of the Prompt Optical Emission from Short GRB.
3. Optical Precursors Detection.
4. Prompt optical polarizations discovery.
5. High time resolution optical observations.

4 The Gamma ray bursts' MASTER earlier observations

The GRB Coordinates Network (GCN) global physical experiment consists of: space gamma (and X-ray) observatories, the gamma-ray center network that accumulates events data and distributes to the ground robotic observatories to give them the possibilities to point and observe the GRB error-boxes as soon as possible, i.e. as close as possible to the trigger time (the main principles are described by Barthelmy 1995).

4.1 MASTER

The Global MASTER Robotic Net is the unique colored twin telescope system with possibility and capability of simultaneous observations in two different filters or in two perpendicular polarizations (BVRI + polarization filters at every MASTER observatory).

MASTER Global Robotic Net (Lipunov et al. 2010, 2016a,b; Kornilov et al. 2012; Gorbovskoy et al. 2013, 2016) consists of identical equipment: wide-field optical channel – twin 40-cm optical robotic telescopes with 8 square degrees field of view up to 20–21 m), and very wide field optical channel with 800 square degrees up to 15 m with the 0.15 s time resolution, located in the following observatories:

MASTER-Amur (longitude 127.483 degree, latitude 50.319 degree), MASTER-Tunka (103.067 , 51.810), MASTER-Ural (59.542, 57.036) and MASTER-Kislovodsk (42.524, 43.7461) located in Russia; MASTER-SAAO (20.811, –32.379) located in South Africa; MASTER-IAC (–16.511, +28.299) located in Spain, Canarias; and MASTER-OAFA (–31.802, –69.000) located in Argentina.

The main advantages of MASTER instruments are the following (Lipunov et al. 2016; Gorbovskoy et al. 2016):

1. The main MASTER unique feature is own software, which was written over the course of 10 years, and which has led us to discover new optical transients in MASTER images within several minutes after readout from the CCD. This information includes the full classification of all sources from the image, the data from previous MASTER-Net archive images for every source, full information from VIZIER database and all open source (e.g., Minor planet checker center), derivation of orbital elements for moving objects and more.

2. MASTER large field of view of 8 square degrees (twin $2.05^\circ \times 2.05^\circ$) of Wide-Field main MASTER-II optical channel (up to unfiltered 20^m per 60–180 s exposition) and 800 square degrees (twin $16^\circ \times 24^\circ$) of Very Wide Field cameras, i.e. MASTER-VWFC (up to 11–12^m per 1 second and 13.5–15^m on sum) at each of MASTER observatories.

3. Twin tubes can observe different fields (that let us observe, for example, FERMI error-boxes in almost real-time).

4. Twin tubes can observe the frame in different polarizations filters and in BVRI.



Figure 9 The statistic of the fraction of the first pointing by MASTER (left figure) and the fraction of the first prompt observations (right figure) in 2010–2011.

5. MASTER has a very fast time positioning system. These telescopes are very suitable for follow-up program, such as prompt optical observations of gamma-ray bursts, neutrino alerts, etc. (see Fig. 9).

All MASTER telescopes have the same optical scheme and set of polarization and BVRI filters, i.e. equipment.

The main purpose of MASTER is to detect prompt GRB emission by rapid response to GRB-alerts (alert-mode observations). The second purpose is the discovery of optical transients of different nature (more than 10) in survey mode and to study the dark energy parameters. The third purpose refers to neutrinos and gravitational waves alerts observations to detect their sources. The fourth is the search for exoplanets, the fifth is the search for unusual moving objects in Solar system, etc.

The unique MASTER key is its own software, which was written during 10 years by the best MSU scientists and programmers. This MASTER software gives us all information about all optical sources at every image after 1 or several minutes (depends on area; the Milky Way needs several minutes) after reading it from CCD. This information includes the full classification of all sources from the image, the data from previous MASTER-Net archive images for every source, full information from VIZIER database and all open sources (for example, Minor planet checker center), orbit elements searching for and detecting moving objects and etc. In search tasks real astrophysical source cannot take a 1, 2 or 4 pixel, because you will never prove, that the new source is real, and not artificial. The real transient must have more than 10 pixels with a specific profile to divide it from the different hot pixels.

The MASTER software discovers the optical transients not by the difference of the previous and current images, but by the full identification of each sources at every image. This MASTER software let us discover 1000 optical transients in fully automatic mode. These optical transients are the following: optical counterpart of gamma-ray bursts; QSO flares; supernovae; novae; dwarf novae (3 types); anti-novae (ϵAuriga type); polars; R CrB and other cataclysmic variables; optical transient with unknown nature (single line in spectrum, Moiseev et al. 2011); asteroids (including potentially hazardous) and comets http://observ.pereplet.ru/MASTER_OT.html).

4.2 The flux calibration

Let us discuss the MASTER flux calibration, see Gorbovskoy et al. (2012).

To convert the BVRI magnitudes into absolute values, we use the zero-magnitude flux densities of the Landolt photometry (see, e.g., Pickles, Depagne 2010). To convert CCD photometry into absolute fluxes without color filter interposed, that is, in a wide waveband (see Fig. 6), we use the Pogson formula relating stellar magnitudes and CCD band-integrated flux with a zero-magnitude flux calculated using the Vega spectrum as given by Hayes (1985). The standard stars are designated with the W and P magnitudes: obtained from observations in the wide wave-band and in the wide waveband plus polarizer. Both are approximated by the formula $W = 0.8R + 0.2B$. This formula is arrived at by compilation of color diagrams W–X versus B–R, where X is a combination of stellar magnitudes, $X = a_R R + b_B B$. In a general case, points group around straight oblique line. The zero-slope of the relation is achieved by fitting for the parameters a_R and b_B. It is found that for white light the above representation of the wide-band magnitudes holds with an accuracy of 4 per cent for W-magnitudes and per cent, for P-magnitudes. Unfortunately, for the polarizer that we used in the observations there was a long-wavelength interval with unspecified transmission efficiency function. Simulating polarizer transmission function in different ways and folding it with different spectra (Vega's, $\propto v^{-1}$, and $\propto v^0$), we have estimated the maximum additional uncertainty of $\sim$20 per cent. Thus we add 20 percent of uncertainty when we convert P to absolute fluxes. Observed magnitude W of an investigated source is converted into the absolute flux values

$$F^W_{\rm GRB} = F^W_\circ \times 10^{-0.4W},$$

where $F^W_\circ$ is the calculated Vega flux in the CCD spectral band:

$$F^W_\circ = \int F_{\rm Vega}(\lambda) W(\lambda) d\lambda = 1.33 \times 10^{-5}\,{\rm erg\,cm^{-2}\,s^{-1}}.$$

In the same way, magnitudes P are converted to flux values using $F^W_{\rm GRB}$ with the zero-magnitude flux

$$F^P_\circ = \int F_{\rm Vega}(\lambda) P(\lambda) d\lambda = 1.16 \times 10^{-5}\,{\rm erg\,cm^{-2}\,s^{-1}}.$$

In the above expressions, $W(\lambda)$ and $P(\lambda)$ are, respectively, the normalized CCD response function and its normalized convolution with the transmission efficiency of the polarizer. Of course, if one observes a source with partly (linearly) polarized light through such polarization filter, full information is needed on the degree of polarization and its angle to derive the total flux. For anpolarized source, or for a source with equal signals from two polarizers (the case of GRB100906A Gorbovskoy et al. 2012), we can safely use this formula. For details see Gorbovskoy et al. (2012). To obtain GRB's flux density at the wavelength of the CCD-response maximum, 5500 Å, we divide flux FW GRB or FP GRB by an effective frequency interval $\Delta\nu_{\rm eff}$ of the corresponding response function. Naturally, the value of $\Delta\nu_{\rm eff}$ depends on a particular spectral distribution. The effective frequency interval of the CCD response function is $\sim 3.9 \times 10^{14}$ Hz, calculated as the mean of values $\Delta\nu_{\rm eff}$ for the Vega spectrum, white light, and power-law spectrum with –1 slope, all falling inside a 15 per cent uncertainty

interval. The effective frequency interval of the CCD plus polarizer, calculated in the same way, is $\sim 3.2 \times 10^{14}$ Hz with a 10 percent uncertainty interval. Bearing in mind that a real spectrum might be something different from the three considered in such simple analysis, we assume approximately a 20 percent accuracy for converting from flux units to spectral flux density units.

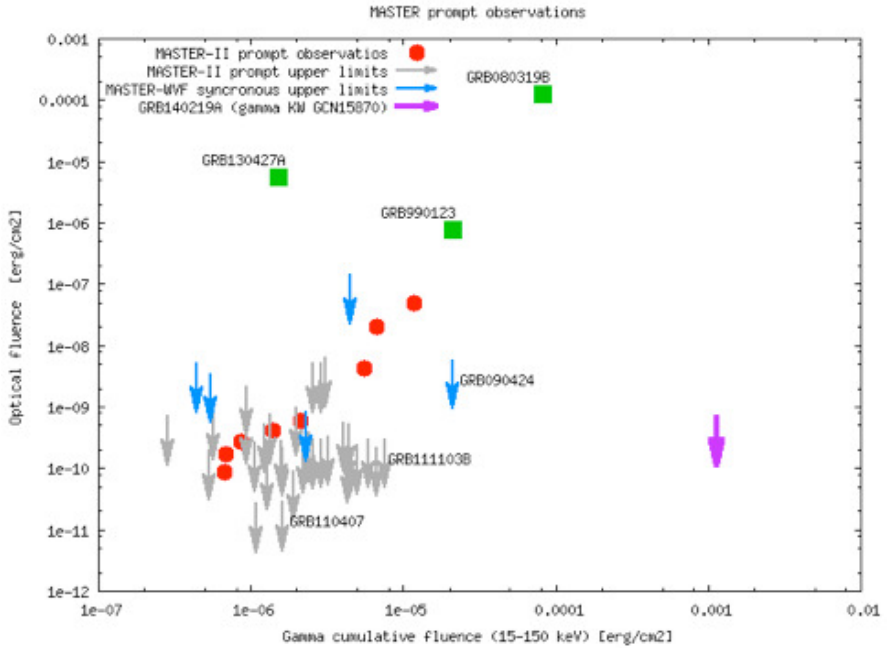


Figure 10 MASTER optical synchronous (prompt) observations of GRBs.

4.3 GRB observation strategy on the example of GRB100901A

Let us see the MASTER Net GRB observations strategy applied to the example of prompt optical observations of GRB 100901A (Gorbovskoy et al. 2012).

The GRB 100901A triggered the Swift Burst Alert Telescope (Swift/BAT) at 13:34:10 UT on September 1, 2010. Time T_{90}, during which 90 per cent of γ-fluence is detected, was 439 ± 33 s (Immler et al. 2010; Sakamoto et al. 2010b). Two MASTER robotic telescopes were pointed to the Swift BAT position of GRB 100901A: at Tunka at 103 s after the BAT trigger time T_0 and near Blagoveschensk, 101 s after T_0 (Ivanov et al. 2010a), see Figs. 11 and 12. We have got more than $\sim$5 min of optical observations simultaneous to the prompt γ-emission of the GRB. The source was too low above the horizon at Tunka, and it was possible to observe it with only one of the optical tubes. The second tube was shadowed by the dome, which made impossible measuring polarized light.

The eastern telescope, near Blagoveschensk, was not operational because of the bad weather conditions. An optical flare, with maximum at 17.0^{m} in the MASTER

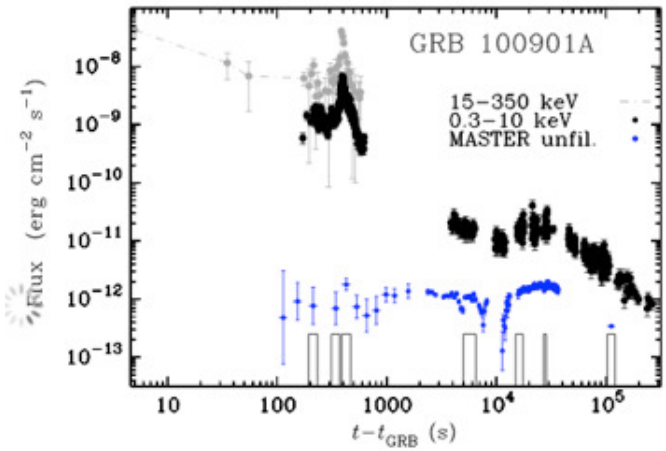


Figure 11 GRB 100901A optical light curve obtained by MASTER (blue points with vertical bars representing errors and horizontal bars representing exposure times; data are corrected for the Galactic extinction) along with the Swift /BAT 15–350 keV flux with 10 s binning (grey dots connected by dot-dashed lines) and Swift /XRT 0.3–10 keV unabsorbed flux (black dots Page, Immler 2010). Thin-line rectangles show the time intervals selected for spectral analysis.

unfiltered band, was clearly detected at 426 ± 40 s after the trigger time (Ivanov et al. 2010b), synchronously with the X-ray flare (Page, Immler 2010) and the γ-flare (Sakamoto et al. 2010b).

The MASTER-Ural telescope (Kourovka) was pointed to GRB100901A ∼5 hours later. Overall, we have been continuously observing the GRB during 14 hours at three sites, Tunka, Ural, and Kislovodsk, in different optical bands: unfiltered, R, I, and V. The 1.5-m telescope at Observatorio de Sierra Nevada, Spain observed the GRB about 11 hours after the trigger (Sanchez-Ramirez et al. 2010). The redshift of the host galaxy $z = 1.408$ was obtained at the 8-m Gemini-North telescope (Chornock et al. 2010).

GRB 100906A

At 13:49:27 UT, September the 6th, GRB 100906A was detected (Markwardt et al. 2010). The BAT/Swift detected several bright peaks with $T_{90} = 1144 \pm 1.6$ s (Barthelmy et al. 2010b). GRB 100906A has been also observed by the Konus–Wind starting from 13:49:30 UT (Golenetskii et al. 2010). Two MASTER telescopes, at Tunka and Blagoveschensk, were pointed to the GRB position, respectively, 38 s after the BAT trigger time T_0 and 58 s after T_0. As a pilot instrument was mounted at the time at the Blagoveschensk site, we present only the data obtained by the telescope at Tunka. In Ural and Kislovodsk, the weather conditions were not suitable for observations.

A bright optical transient was localized by MASTER at the Swift /UVOT position (Markwardt et al. 2010), 13 mag at maximum. During the first hour after the trigger

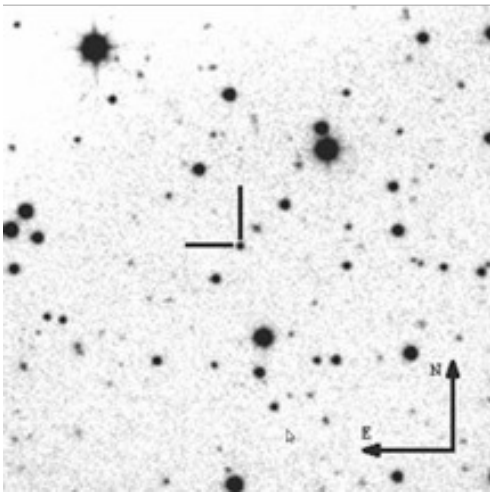


Figure 12 The optical source of GRB100901A.

time, 24 images in unfiltered light at two polarization angles were produced by the Tunka telescope. We show the early observations of GRB 100906A in optical, 0.3–10 keV, and 15–150 keV energy range, see Figs. 13, 14. A movie of the optical burst of GRB 100906A as seen at Tunka is available on the web. We calculate the relative difference between the signals coming from the two polarization filters, for the time interval 100–10^4 s after T_0. It is less than the relative measuring accuracy of filters 2 per cent, estimated through the observations of standard stars. Unfortunately, technical limitations do not allow us to draw a decisive conclusion about the polarization degree of GRB 100906A. The 1.5-m OSN telescope at Sierra Nevada observed the GRB few hours after T_0. Calibration for BV and IR bands is done using 49 USNO stars, and for U-band using a Landolt star observation. Aperture photometry is carried out using phot as implemented in IRAF with a radius equal to the seeing. The

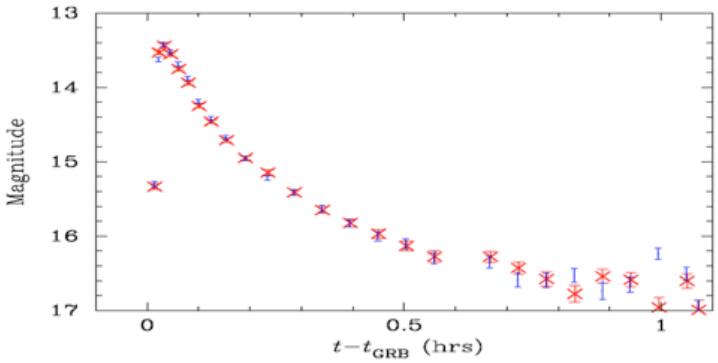


Figure 13 MASTER light curve of GRB 100906A in two polarizations, unfiltered band (blue dots and red crosses). Data are not corrected for the Galactic extinction.

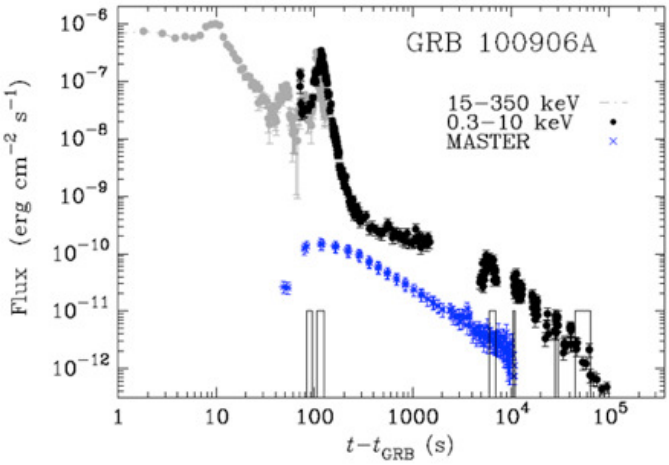


Figure 14 GRB 100906A optical light curve obtained by MASTER with one polarization filter (blue dots with 20 per cent error bars resulted due to uncertainty of magnitude-flux conversion, see Section 3.2; data are corrected for the Galactic extinction) along with the Swift/BAT 15–350 keV flux with 1 s binning (grey dots connected with dot-dashed line; data with negative lower limits are not shown) and the Swift/XRT 0.3–10 keV unabsorbed-flux light curve (black dots; Beardmore, Markwardt 2010). Thin-line rectangles show the time intervals selected for spectral analysis.

error of the afterglow magnitude was obtained adding quadratically the statistical error given by phot and the zero point error determined with the 49 field reference stars. The redshift of the host galaxy $z = 1.727$ was obtained with the Gemini-North telescope (Tanvir et al. 2010).

The prompt behavior of the two closely studied GRBs is quite distinct. For GRB 100901A, we see a similarity of light curves in the optical, γ, and X-rays at around 300–500 s after the trigger. For GRB 100906A, such similarity of temporal behaviour is absent. It has a perfectly smooth optical light curve, gradually rising and decaying, a different profile from that in the 15–150 keV band.

From this point of view, GRBs 100901A and 100906A support the earlier noticed diversification for optical emission detected during the first few minutes after the onset of a GRB (e.g., Vestrand et al. 2005, 2006): in some cases the prompt optical flux variations are correlated with the prompt γ-emission, and in other cases early optical afterglow light curve is uncorrelated with the γ-ray light curve. Such division of GRBs can be understood within the picture of the optical emission generated from different sites of the relativistic jet: in the internal, external forward, or reverse shock waves (e.g., Sari, Piran 1999; Meszaros, Rees 1999). The external forward shocks arise due to the interaction of the ejected material with the ISM and propagate into the ambient media, the reverse shock propagates into the ejecta itself, and the internal shocks are produced because of the collisions among many engine-ejected shells (e.g., Meszáros, Rees 1997; Sari, Piran 1997). The correlation between the optical, γ, and X-rays can be achieved, if the optical emission is produced by the synchrotron mechanism within the same region as the hard radiation. The early X-ray and soft γ-ray spectrum of

GRB 100901A shows a dependence close to $\nu-1/2$, which is typical for the synchrotron radiation if $\nu_c < \nu < \nu_m$ (where ν_m and ν_c are the characteristic synchrotron and cooling frequencies, respectively) in the regime when electrons lose energy very quickly (see, e.g., Sari, Piran, Narayan 1998; Sari, Piran 1999). Adding the MASTER optical point (corrected for the Galaxy extinction), and fitting simultaneously the optical, 0.3–10 keV, and 15–150 keV data by an absorbed power law, we can determine the magnitude of the optical extinction in the host.

We should add that the data can also be reconciled with the prompt spectral distributions of GRB 100901A peaking between the optical and X-rays, if $\nu_{\rm opt} < \nu_c < \nu_x$. Then, a migration of the cooling frequency ν_c ($\propto t - 1/2$, see, for example, Sari, Piran, Narayan 1998) may be hidden in the errors of resulting $A_V^{\rm int}$. Spectral fitting of an absorbed power law to the late-time MASTER and 0.3–10 keV data provides $A_V^{\rm int} = 0.45 \pm 0.15$, lower than $A_V^{\rm int} = 0.8 \pm 0.1$ for the prompt fits (values are for the SMC type of the extinction law; see Section 4.2). This could be a confirmation of the above suggestion, but a detailed discussion is beyond the aims of the present study.

In contrast to the above picture, GRB 100906A exhibits no correlation between the optical and high energy emission at 15–150 keV. We suggest that in this case the optical radiation originates at the front of the external shock, and the light curve shows a smooth conversion of a bow shock to a self-similar mode of the afterglow with a power decay $F_{\rm opt} \propto t^{-\alpha}$ with $\alpha = 1.08 \pm 0.01$.

A critical test for determining the site of the optical emission could be the observation of polarization. If radiation in the internal shock occurs in the ordered magnetic field, some polarization is expected (see, e.g., Steele et al. 2009). This implies that the magnetic field coherence scale is larger than the size of the visible emitting region. Thus, a discovery of a considerable (>10%) polarization of the optical radiation, correlating with the prompt γ-ray emission, would be strong evidence in favor of the optical radiation originating in the internal shock. Conversely, the afterglow radiation from the external shock occurs in the chaotic field of the interstellar medium compressed by the shock and should not have a considerable polarization (Gruzinov, Waxman 1999). Low degree of polarization of the optical light would rule out the presence of a large-scale ordered magnetic field in the emitting region (Mundell et al. 2007).

For the observations of GRB 100906A, we can infer that in the time interval from 100 s to ∼1 h the degree of linear polarization of the optical emission is less than 10% with probability of about 60 per cent.

So the resumé is the following: for two sources, GRB 100901A and GRB 100906A, we detected optical counterparts and obtained light curves starting before cessation n of γ-ray emission, at 113 s and 48 s after the trigger, respectively.

4.4 Earlier optical linear polarization observations on the example of GRB 150301B and GRB 150413A

In 2015 MASTER Global Robotic Net reported the early optical linear polarization observations of two gamma-ray bursts GRB 150301B and GRB 150413A (Figs. 15, 16), see Gorbovskoy et al. (2016). We found the minimum polarization for GRB 150301B to be 8 per cent at the beginning of the initial stage, whereas we detected no polarization for GRB 150413A either at the rising branch or after the burst reached



Figure 15 MASTER-Tunka unfiltered discovery and at maximum of light curve images of GRB150413A.



Figure 16 MASTER-SAAO discovery images of GRB150301B, expositions 10 s both tubes in perpendicular polarization filters.

the power-law afterglow stage. This is the earliest measurement of the polarization (in cosmological rest frame) of gamma-ray bursts. The primary intent of the paper is to discover optical emission and publish extremely rare (unique) high-quality light curves of the prompt optical emission of gamma-ray bursts during the non-monotonic stage of their evolution. We report that our team has discovered the optical counterpart of one of the bursts, GRB 150413A.

5 Conclusions

In this paper we have discussed unsolved GRB theoretical (the nature of this most powerful phenomenon in the Universe) and observational (strategy and difficulties of prompt and earlier observations) problems, and also discussed first key steps in GRB investigations, and GRB observation strategy on the example of GRB 100901A and GRB 100906A with optical counterparts, discovered by MASTER Global Robotic Net, and demonstrated the earlier optical linear polarization observations on the example of GRB 150301B and GRB 150413A, also discovered by MASTER.

Acknowledgements

This work was partially supported by Russian Science Foundation 16-12-00085 and Russian Foundation of Basic Research 15-02-07875.

REFERENCES

Strong I.B., Klebesadel R.W., Olson R.A. (1974) ApJ, 188, L1
Klebesadel et al. (1973) ApJ, 182, L85
Mazets E.P., Golenetskii S., Il'inski V.N. (1974) Pis'ma v ZhETF, 19, 126
Mazets, E.P., Golenetskii, S.V. (1981) Astrophys. Space Phys. Rev., 1, 205
Mazets E., Golenetskii S. (1988) Soviet Scientific Reviews, Sec. E, Astrophys. Space Phys. Rev., 6, 3, 283
Mazets E.P. (1988) Astrophys. Space Phys. Rev., 6, 281
Mazets E., Golenetskii S. et al. (1987) ICRC, 2, 284
Aptekar' R.L., Golenetskii S.V., Mazets E.P. et al. (2010) Usp. Fiz. Nauk, 180, 420
Lipunov V.M. et al. (1995) ApJ, 454, 593
Lipunov V.M., Postnov K.A., Prokhorov M.E. (1996) A&A, 310, 489 (The "Scenario Machine": restrictions on key parameters of binary evolution)
Lipunov V.M., Postnov K.A., Prokhorov M.E., Bogomazov A.I. (2009) ARep, 53, 915 (Description of the "Scenario Machine")
Costa E. et al. (1997) IAU Circular 6584
Groot P.J. et al. (1997a) IAU Circular 6574
Groot P.J. et al. (1997b) IAU Circular 6584
Kulkarni S.R. et al. GCN-04 http://gcn.gsfc.nasa.gov/gcn3/neg4.gcn3
Bloom J.S., Djorgovski S.G., Kulkarni S.R. (2001) ApJ, 554, 678
Bond H. E. (1997) IAU Circular 6654 http://www.cbat.eps.harvard.edu/iauc/06600/06654.html
Castro-Tirado A., Gorosabel J. et al. (1998) Science, 279, 5353
Akerlof C.W., McKay T.A. (1999a) The GRB Coordinates Network Circular, No. 205, #1 http://gcn.gsfc.nasa.gov/gcn/gcn3/205.gcn3
Akerlof C.W., Balsano R. et al. (1999b) Nature, 398, 400
Akerlof C.W. et al. (2000) ApJ. Lett., 532, L25
Bisnovatyi-Kogan G.S., Blinnikov S.I., Zaharov A.F. (1984) Astron. Zh., 61, 104
Paczynski B. (1986) ApJ, 308, L43
Woosley S.E. (1993) ApJ, 405, 273
Hoyle F., Fowler W.A. (1963) Nature, 197, 533
Hoyle F., Fowler W.A. (1963) MNRAS, 125, 169
Ozernoy L. (1966) Sov. Phys. Doklady, 10, 581
Ozernoy L. (1966) Sov. Astr., 10, 241
Morrison P. (1969) ApJ, 157L, 73
Ozernoy L., Usov V. (1973) Ap&SS, 25, 149
Bisnovatiy-Kogan, G.S. (1971) SvA, 14, 652
LeBlanc J. M., Wilson J.R. (1970) ApJ, 161, 541
Lipunov V.M. (1983) A&A, 127L, 1

Ostriker J.P. (1973) BAAS, 5, 29
Lipunov V.M. (1987) AZh, 64, 203
Lipunova G.V. (1997) Astronomy Letters 23, 84
Lipunova G.V., Lipunov V.M., (1998) Astron. Astrophys., 329, L29
Lipunov V.M., Gorbovskoy E.S. (2007) ApJLetters, 665, 97
Troja E. et al. (2007) ApJ, 665, 599
Lipunov V.M., Gorbovskoy E. S. (2008) MNRAS, 383, 1397
Lipunov V. et al., (2016a) MNRAS, 455, 712
Lipunov V., Gorbovskoy E., Afanasiev V. et al. (2016b) A&A, 588, 90
Gorbovskoy E., Lipunov V., Buckley D. et al. (2016) MNRAS, 455, 312
Bogomazov A.I., Lipunov V.M., Tutukov A.V. (2007) ARep, 51, 308
Koshut Th.M. et al. (1995) ApJ, 452, 145
Kardashev N.S. (1995) MNRAS, 276, 515
Barthelmy S. et al. (1995) Astrophysics and Space Science, 231, 235
Lipunov V.M. (2010) IAC Talks, Astronomy and Astrophysics Seminars from the Instituto de Astrofisica de Canarias, 78
Kornilov V.G. (2012) MNRAS, 425, 1549
Gorbovskoy E.S. (2013) ARep, 57, 233
Moiseev et al. (2011) Astron. Telegram 3255, 1
Pickles A., Depagne E. (2010) PASP, 122, 1437
Hayes D.S. (1985) IAUS, 111, 225
Gorbovskoy E.S., Lipunova G.V., Lipunov V. M. et al. (2012) MNRAS, 421, 3, 1874
Immler S. et al. (2010) GCNR, 304, 1
Sakamoto T. et al. (2010) GCN, 11169, 1
Ivanov K. et al. (2010a) GCN, 11163, 1
Ivanov K. et al. (2010b) GCN, 11161, 1
Page K.L., Immler S. (2010) GCN, 11171, 1
Sakamoto T. et al. (2010b) GCN, 11169, 1
Sanchez-Ramirez R. et al. (2010) GCN, 11180, 1
Chornock et al. (2010) GCN, 11164, 1
Markwardt C.B. et al. (2010) GCN, 11227, 1
Markwardt C.B. et al. (2010) GCN, 11486, 1
Barthelmy S.D. et al. (2010b) GRB Coordinates Network, Circular Service, 11233, 1
Golenetskii S. et al. (2010) GCN, 11251, 1
Markwardt C.B. et al. (2010) GCN, 11332, 1
Tanvir N. R., Wiersema K., Levan A.J. (2010) GRB Coordinates Network, Circular Service, 11230, 1
Beardmore A.P., Markwardt C.B. (2010) GRB Coordinates Network, Circular Service, 11244, 1
Vestrand W. T. et al. (2005) Nature, 435, 178
Vestrand W. T. (2005) Bulletin of the American Astronomical Society, 37, 1187
Vestrand W.T. et al. (2006) Nature, 442, 7099, 172
Sari R., Piran T. (1999) A&AS, 138, 537
Meszaros P., Rees, M.J. (1999) MNRAS, 306, 3, L39
Meszaros P., Rees M.J. (1997) ApJ, 476, 1, 232
Sari R., Piran, T. (1997) ApJ, 485, 1, 270
Sari R., Piran T., MNRAS, 287, 1, 110

Sari R., Piran T., Narayan R. (1998) AIPC, 428, 704
Sari R., Piran T. (1999) A&AS, 138, 537
Gruzinov A., Waxman E. (1999) ApJ, 511, 852
Mundell C.G. et al. (2007) Science, 315, 5820, 1822